Journal of ELECTRONIC MATERIALS, Vol. 46, No. 4, 2017
DOI: 10.1007/s11664-016-5148-3
© 2016 The Minerals, Metals & Materials Society

CrossMark

Influence of Thermal Annealing Treatment on Bipolar Switching Properties of Vanadium Oxide Thin-Film Resistance Random-Access Memory Devices

KAI-HUANG CHEN,[1,6] CHIEN-MIN CHENG,[2] MING-CHENG KAO,[3] KUAN-CHANG CHANG,[4] TING-CHANG CHANG,[5] TSUNG-MING TSAI,[4] SEAN WU,[1] and FENG-YI SU[2]

1.—Department of Electronics Engineering and Computer Science, Tung-Fang Design Institute, Kaohsiung, Taiwan. 2.—Department of Electronic Engineering, Southern Taiwan University of Science and Technology, Tainan, Taiwan. 3.—Department of Electronic Engineering, Hsiuping University of Science and Technology, Taichung, Taiwan, ROC. 4.—Department of Materials and Optoelectronic Science, National Sun Yat-Sen University, Kaohsiung, Taiwan. 5.—Department of Physics, National Sun Yat-Sen University, Kaohsiung, Taiwan. 6.—e-mail: d9131802@gmail.com

The bipolar switching properties and electrical conduction mechanism of vanadium oxide thin-film resistive random-access memory (RRAM) devices obtained using a rapid thermal annealing (RTA) process have been investigated in high-resistive status/low-resistive status (HRS/LRS) and are discussed herein. In addition, the resistance switching properties and quality improvement of the vanadium oxide thin-film RRAM devices were measured by x-ray diffraction (XRD) analysis, x-ray photoelectron spectrometry (XPS), scanning electron microscopy (SEM), atomic force microscopy (AFM), and current–voltage (*I*–*V*) measurements. The activation energy of the hopping conduction mechanism in the devices was investigated based on Arrhenius plots in HRS and LRS. The hopping conduction distance and activation energy barrier were obtained as 12 nm and 45 meV, respectively. The thermal annealing process is recognized as a candidate method for fabrication of thin-film RRAM devices, being compatible with integrated circuit technology for nonvolatile memory devices.

Key words: Thermal annealing process, bipolar switching properties, vanadium oxide, thin film, RRAM, RTA

INTRODUCTION

Many volatile and nonvolatile memory devices, such as static random-access memory (SRAM), dynamic random-access memory (DRAM), ferroelectric random-access memory (FeRAM), magnetron memory (MRAM), phase-change memory (PCM), and flash memory, are widely used and discussed for application in various portable memory cards and electrical devices. Resistance random-access memory (RRAM) devices are also investigated and discussed due to their excellent nonvolatility characteristics, long retention cycles, high storage capacity, low power consumption, and high readout speed.[1–8]

However, the complex composition of the electrical materials used in RRAM devices as well as their fabrication cost prevent their consideration and selection for use in volatile memory.[9,10] Simple binary metal oxide materials have also been widely considered and investigated for application in various Nd_2O_3, W_2O_3, ZnO, and Ta_2O_5 thin-film RRAM devices.[11–15] For contacts with low ohmic resistance and excellent structural properties, platinum electrodes are necessary for electrical thin films and must be used for metal–insulator–metal (MIM) RRAM devices.[16]

(Received February 16, 2016; accepted November 16, 2016; published online December 1, 2016)

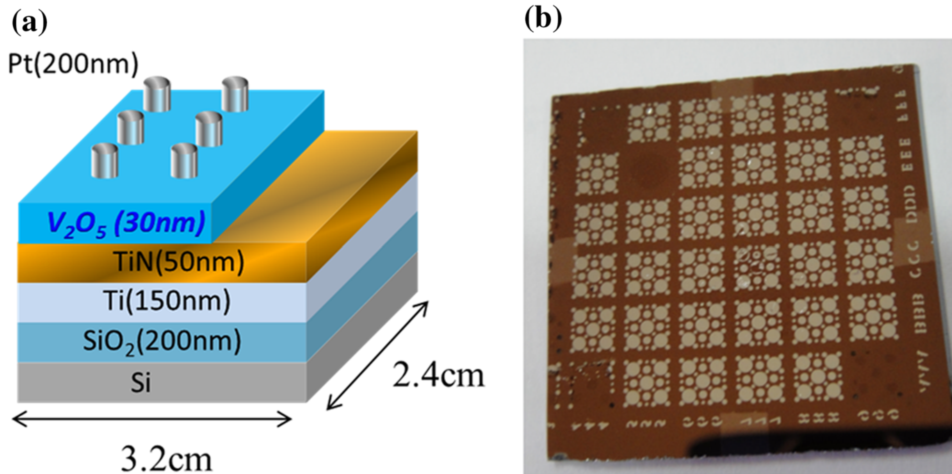

Fig. 1. Vanadium oxide thin-film RRAM devices: (a) metal–insulator–metal (MIM) structure, and (b) plan-view morphology.

The treatment cost and simple reaction process of rapid thermal annealing technology make it an essential technology for recrystallization of oxide materials.[4] In this work, we investigated the bipolar resistive switching properties of the Pt/V_2O_5/TiN structure, i.e., TiN bottom electrode, vanadium oxide film, and Pt top electrode. Moreover, the LRS/HRS of RRAM devices based on vanadium oxide thin film prepared using thermal annealing treatment were also investigated and are discussed below.

EXPERIMENTAL PROCEDURES

Samples with the MIM structure shown in Fig. 1a were prepared using sputtering technology to investigate the bipolar switching properties of such RRAM devices. A vanadium oxide target was placed 5 cm away from the substrate, and radio frequency (RF) sputtering power of 160 W was applied. After deposition at room temperature, the as-deposited vanadium oxide thin film was treated by rapid temperature annealing (RTA) at 450–550°C for 30 s in air. To complete the MIM structure, an array of circular top contacts with diameter of 50 μm was formed by deposition of Pt film with thickness of 200 nm using direct-current (DC) sputtering technology at 5×10^{-5} Torr. The bipolar switching properties of the resulting RRAM devices were determined using an Agilent B1500 semiconductor parameter analyzer. To investigate the effect of the thermal annealing treatment on the vanadium oxide thin film, the physical properties were determined and analyzed using SEM, XPS, and XRD measurements.

RESULTS AND DISCUSSION

To determine the HRS/LRS properties for the 5-V forming process, the *I–V* switching curves of a vanadium oxide thin-film RRAM device are shown in Fig. 2a. The compliance current was 10 mA. In the SET process, the RRAM device was transferred to the LRS by applying a high positive bias compared with the SET voltage. In the RESET process, a continuous decrease of the operating current in the LRS transferred the device to the HRS for an applied negative bias above the RESET voltage.

Figure 2 presents 100 cycles of *I-V* switching for RRAM devices with nontreated and RTA treated vanadium oxide thin film. The operating current in the LRS was slightly increased for the RRAM device with the annealed vanadium oxide thin film. This is due to the decreased defects and dangling bonds in the vanadium oxide thin film after annealing. In previous study, the electrical properties of thin films deposited at different oxygen concentrations revealed different resistive switching and leakage current properties.[17]

The XPS results (Fig. 2b) showed that the V $2p^{3/2}$ and oxygen 1*s* corresponding to dangling bonds were shifted to higher binding energy for the annealed thin film. The operating current of the annealed thin-film RRAM in LRS was slightly increased and the oxygen vacancy efficiency decreased by the RTA process. For a 0.5-V reading voltage (Fig. 2), the ON/OFF ratio for the annealed RRAM devices was larger than for the nontreated devices. The electron transport mechanism of the nontreated and annealed thin-film RRAM devices is analyzed below by fitting the *I–V* curves.

Figures 3 and 4 depict the surface microstructure morphology of the nontreated and treated RTA thin film as obtained by SEM and AFM, respectively. The nontreated thin film exhibited faceted and inhomogeneous grains (Fig. 3a). The grains and microstructure of the annealed thin films showed large size (Fig. 3b). In AFM images, nonuniform surface roughness and grain size of the thin films were observed. The grain size and microstructure of the annealed thin film were larger than for the nontreated thin film (Fig. 4a, b). Besides, the physical properties of the annealed thin film were

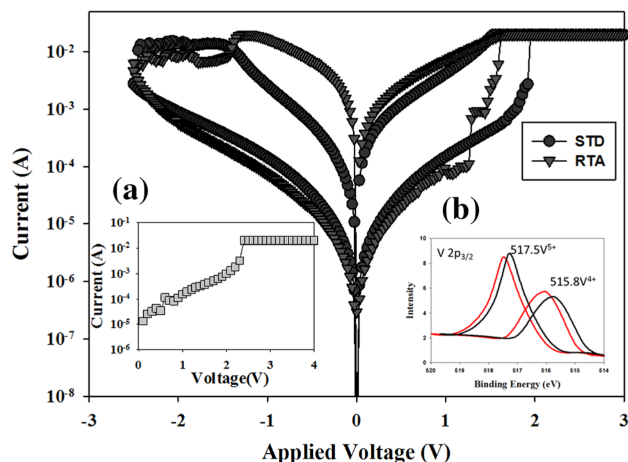

Fig. 2. Typical *I–V* characteristics of nontreated and RTA-treated vanadium oxide thin-film RRAM devices, plus (a) initial forming process, and (b) XPS analysis.

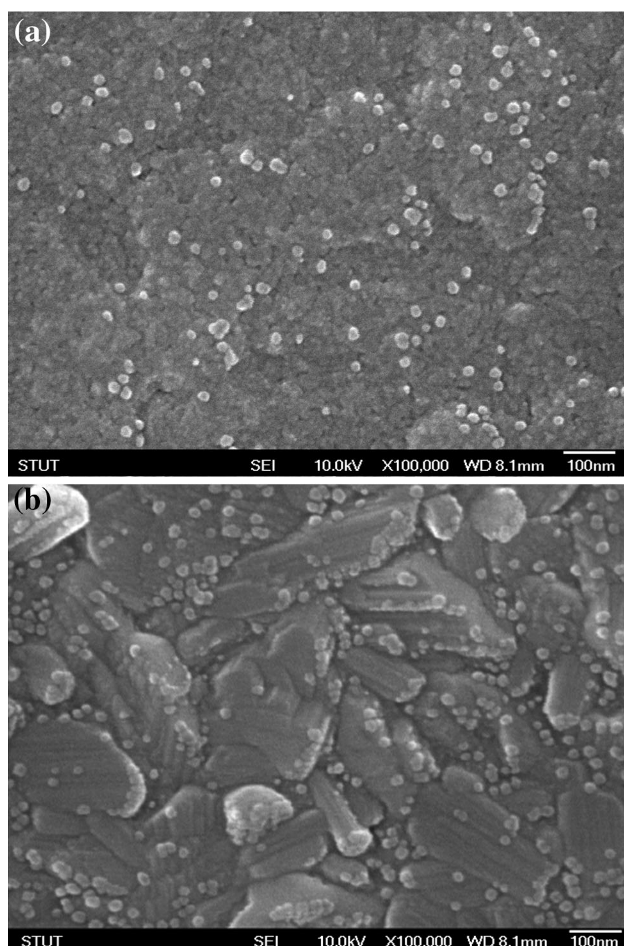

Fig. 3. SEM morphology of (a) nontreated and (b) RTA-treated thin films.

efficiently improved by the thermal annealing treatment.

Figure 5 depicts the XRD patterns of the nontreated and annealed thin film. The (110), (312), and (402) peaks of polycrystalline structure were observed for thin film treated at 500°C. The preferred (110) peak intensity was higher and the full-width at half-maximum (FWHM) narrowest for the annealed thin films. The grain size of the nontreated and annealed thin film was calculated using the simplified Scherrer equation (Fig. 3). In addition, the metal–insulator transition (MIT) of the annealed thin films exhibited an orthorhombic layered structure with lattice parameters of $a = 11.54$ Å, $b = 3.57$ Å, and $c = 4.38$ Å. For increased annealing temperature, the strain parameters of the lattice slightly decreased to -0.015 ($\text{line}^{-2}\ \text{m}^{-4}$) as the c/a lattice parameters decreased. For increasing annealing temperature, the (110) peak shifted slightly to higher diffraction angle, indicating improved crystal quality and lattice strain relaxation.

In previous study, the crystalline grain structure, dielectric constant, and leakage current density of as-deposited thin films showed an apparent improvement after an oxygen annealing process. The decrease of the leakage current density for the annealed thin films is due to the effective decrease of oxygen defects and vacancies by the oxygen annealing process.[18–20]

Compared with ZnO thin films, the carrier concentration of the vanadium oxide thin films was increased to the range of $10^{16}\ \text{cm}^{-3}$ to $10^{18}\ \text{cm}^{-3}$ as the annealing temperature was increased.[21] This increase in carrier concentration is caused by desorption of oxygen molecules from grain boundaries for the thermally annealed thin films. Above annealing temperature of 500°C, the carrier concentration became low because of reformation of the vanadium oxide structure according to the XRD and SEM results. The carrier concentration of the thin film annealed at 500°C was about $4 \times 10^{18}\ \text{cm}^{-3}$ and the resistivity was about 20 Ω cm.

The equation for Schottky emission is

$$J = A^{*}T^{2}\exp\left[-q\left(\Phi_{\mathrm{B}} - \sqrt{\frac{qE_{\mathrm{i}}}{4\pi\varepsilon_{\mathrm{i}}}}\right)/kT\right], \qquad (1)$$

where T is the absolute temperature, Φ_{B} is the Schottky barrier height, ε_{i} is the insulator permittivity, k is Boltzmann's constant, and A^{*} is the Richardson constant. Figure 6a shows the ln I–$V^{1/2}$ curve for the Schottky conduction emission model of the nontreated vanadium oxide RRAM device in LRS state. The ln I–V curve of the RTA-treated thin film RRAM devices in Fig. 6b shows the hopping conduction model at high operating current. The hopping conduction mechanism is due to electrons in shallow traps jumping over an activation energy barrier to form a leakage current along conduction paths formed by metallic filaments.

Figure 7a depicts the ln(I/V)–$V^{1/2}$ curves for nontreated vanadium oxide RRAM devices in HRS. The ln(I/V)–$V^{1/2}$ curve of the nontreated thin films

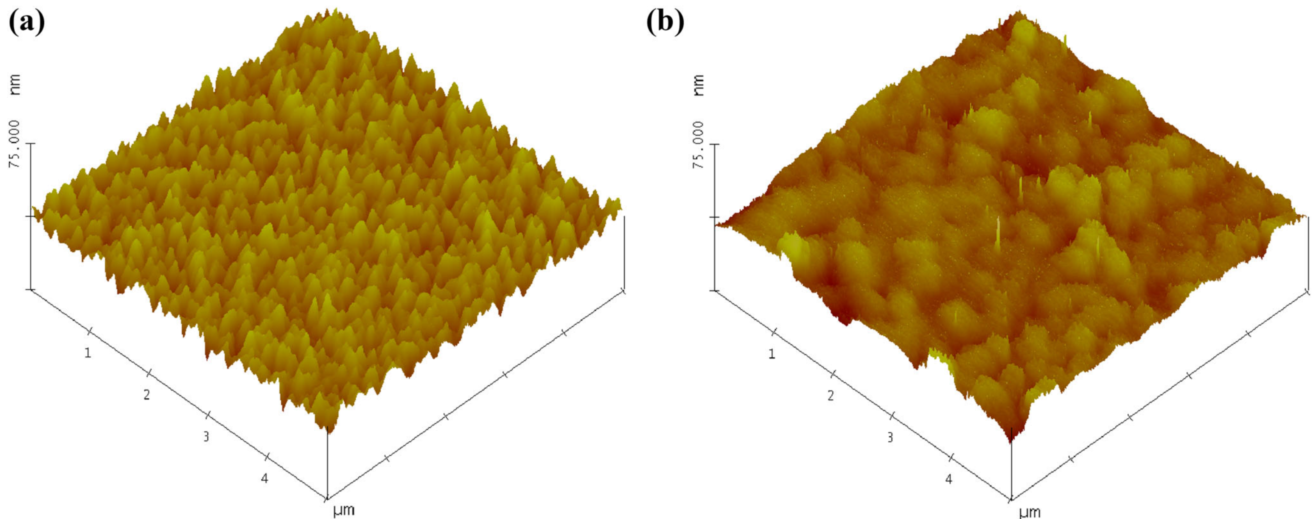

Fig. 4. AFM patterns of (a) nontreated and (b) RTA-treated thin film.

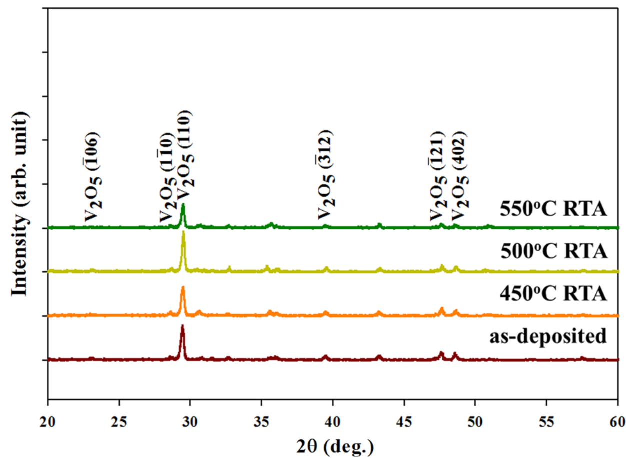

Fig. 5. XRD patterns of nontreated and RTA-treated thin films.

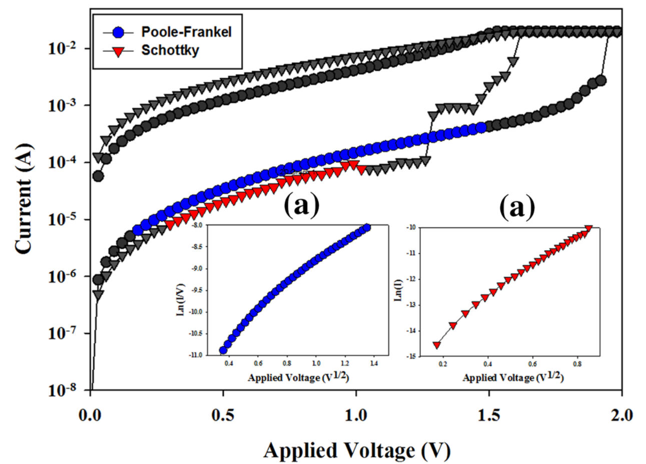

Fig. 7. *I*–*V* curves of RTA-treated vanadium oxide thin-film RRAM devices in HRS: (a) ln(*I*/*V*)–$V^{1/2}$ curves and (b) ln *I*–$V^{1/2}$ curves.

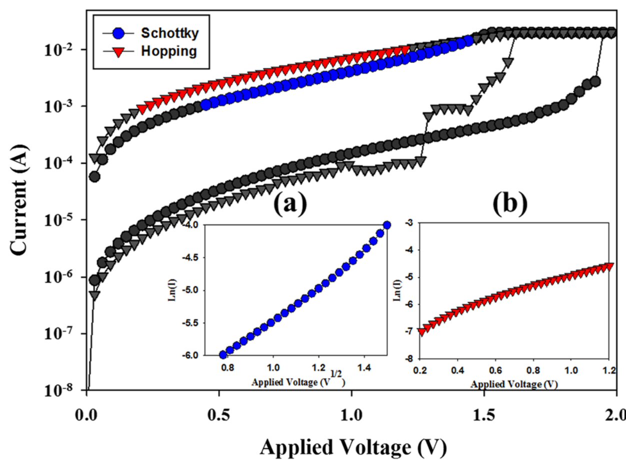

Fig. 6. *I*–*V* curves of RTA-treated vanadium oxide thin-film RRAM devices in LRS: (a) ln *I*–$V^{1/2}$ curves and (b) ln *I*–*V* curves.

followed the Poole–Frenkel emission model. Figure 7b shows that the RTA-treated thin films exhibited the Schottky conduction emission model with lower leakage current. According to fitting of the conduction mechanism, the defect and oxygen vacancy were decreased for the as-deposited vanadium oxide thin film after the thermal annealing process.

To obtain the activation energy (E_a) for the hopping conduction mechanism, the *I*–*V* switching curve of the vanadium oxide RRAM devices was measured at different temperatures.[11] The associated Arrhenius plot equation is

$$E_a = \frac{\partial \log I}{\partial (1/kT)}, \quad (2)$$

where E_a is the activation energy, k is Boltzmann's constant, and T is absolute temperature. To

investigate the metal clustering reaction responsible for the initial formation of metallic filament conduction paths, the hopping conduction activation energy and intertrap separation (Δz) of the thin-film RRAM devices were calculated using the Arrhenius equation:

$$E_a = \frac{\partial \log I}{\partial (1/kT)} = E_C - E_F - qV_A \frac{\Delta z}{2u_a}, \quad (3)$$

where z is the average intertrap separation and u_a is the film thickness.[15] All the ln I–$(1/kT)$ curves exhibited a linear downward trend corresponding to the hopping conduction mechanism. The inset of Fig. 8 shows all the E_a–V curves for the RRAM devices with annealed vanadium oxide thin film to calculate the hopping conduction distance. The activation energy (E_a) and average intertrap separation (Δz) were found to be 45 ± 1.5 meV and 12 ± 1.0 nm, respectively.

In the model for formation of metallic filaments, the metallic element separates and clusters into conduction paths in the thin film, as illustrated in Fig. 9. Figure 9a shows a metallic filament in the RTA-treated vanadium oxide thin-film RRAM device for low applied voltage, exhibiting the hopping conduction mechanism. Electrons are transferred by jumping between shallow defects across an energy barrier, resulting in an electrical current. Figure 9b shows the initial metallic filament path in a nontreated thin-film RRAM device for deep defects according to the Schottky conduction mechanism.

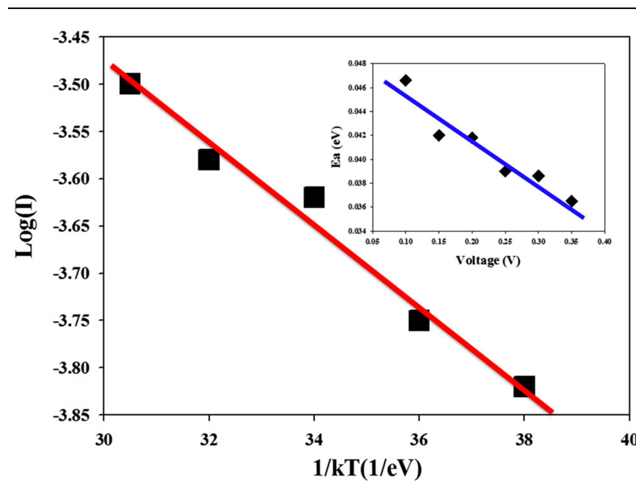

Fig. 8. ln I–$(1/kT)$ curves and E_a–V curves of RTA-treated vanadium oxide thin-film RRAM devices.

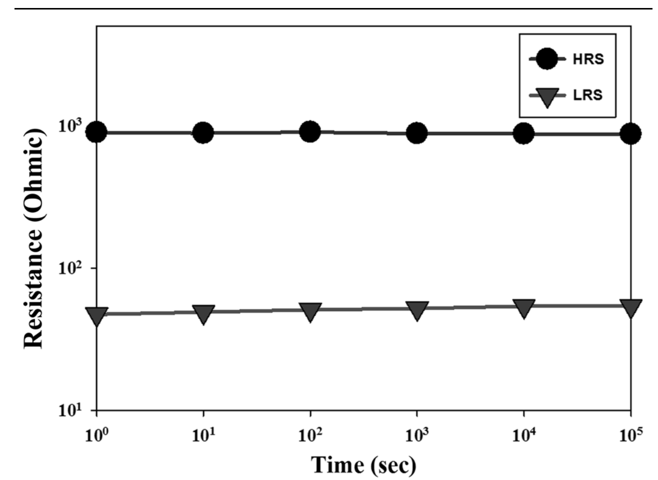

Fig. 10. Retention characteristics of RTA-treated vanadium oxide thin-film RRAM devices at room temperature as measured at 0.5 V.

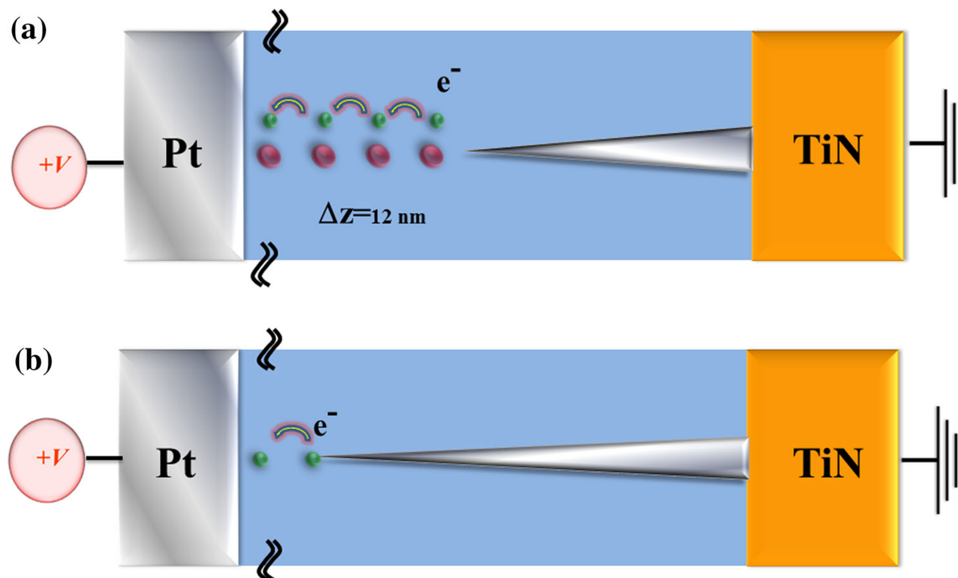

Fig. 9. Electron transfer mechanism and initial metallic filament path for (a) RTA-treated and (b) nontreated vanadium oxide thin-film RRAM devices in SET state.

Switching cycle testing measurements are also useful for characterization of reliability and retention. To determine the performance of such devices for use in nonvolatile random-access memory, the ON/OFF retention characteristics were measured in HRS/LRS. The results (Fig. 10) revealed no significant change in stability during ON/OFF switching cycle testing of an RTA-treated thin-film RRAM device in HRS/LRS over more than 1 year.

CONCLUSIONS

The initial metallic filament formation process, bipolar switching properties, and electrical conduction mechanism of annealed vanadium oxide thin-film RRAM devices in HRS/LRS state are discussed and explained based on an appropriate model for the electron transport path. Improved, low operating current was also achieved in the annealed vanadium oxide thin-film RRAM devices after the thermal annealing process. The nontreated and annealed vanadium oxide thin-film RRAM devices in LRS followed the Schottky conduction emission model and the hopping conduction model, respectively. Finally, the metal atom clustering reaction in the initial metallic filament formation process was investigated based on the hopping conduction energy and average intertrap separation for the RRAM devices.

ACKNOWLEDGEMENTS

The authors acknowledge financial support from the National Science Council of the Republic of China (103-2633-E-272-001).

REFERENCES

1. C.T. Tsai, T.C. Chang, P.T. Liu, P.Y. Yang, Y.C. Kuo, K.T. Kin, P.L. Chang, and F.S. Huang, *Appl. Phys. Lett.* 91, 012109 (2007).
2. C.T. Tsai, T.C. Chang, K.T. Kin, P.T. Liu, P.Y. Yang, C.F. Weng, and F.S. Huang, *J. Appl. Phys.* 103, 074108 (2008).
3. M.C. Chen, T.C. Chang, S.Y. Huang, K.C. Chang, H.W. Li, S.C. Chen, J. Lu, and Y. Shi, *Appl. Phys. Lett.* 94, 162111 (2009).
4. K.H. Chen, T.C. Chang, G.C. Chang, Y.E. Hsu, Y.C. Chen, and H.Q. Xu, *Appl. Phys. A Mater. Sci. Process.* 99, 291 (2010).
5. P.C. Yang, T.C. Chang, S.C. Chen, Y.S. Lin, H.C. Huang, and D.S. Gan, *Electrochem. Solid State Lett.* 14, 93 (2011).
6. Y.E. Syu, T.C. Chang, T.M. Tsai, Y.C. Hung, K.C. Chang, M.J. Tsai, M.J. Kao, and S.M. Sze, *IEEE Electron Device Lett.* 32, 545 (2011).
7. L.W. Feng, C.Y. Chang, Y.F. Chang, W.R. Chen, S.Y. Wang, P.W. Chiang, and T.C. Chang, *Appl. Phys. Lett.* 96, 052111 (2010).
8. L.W. Feng, C.Y. Chang, Y.F. Chang, T.C. Chang, S.Y. Wang, S.C. Chen, C.C. Lin, S.C. Chen, and P.W. Chiang, *Appl. Phys. Lett.* 96, 222108 (2010).
9. K.H. Chen, Y.C. Chen, C.F. Yang, and T.C. Chang, *J. Jpn. Appl. Phys.* 46, 4197 (2007).
10. F.W. Yang, K.H. Chen, C.M. Cheng, and F.Y. Su, *Ceram. Int.* 39, S729 (2013).
11. K.C. Chang, T.M. Tsai, T.C. Chang, Y.E. Syu, and C.C. Wang, *Appl. Phys. Lett.* 99, 263501 (2011).
12. K.C. Chang, T.M. Tsai, T.C. Chang, Y.E. Syu, K.H. Liao, S.L. Chuang, C.H. Li, D.S. Gan, and S.M. Sze, *Electrochem. Solid-State Lett.* 15, 3 (2012).
13. T.M. Tsai, K.C. Chang, T.C. Chang, Y.E. Syu, K.H. Liao, B.H. Tseng, and S.M. Sze, *Appl. Phys. Lett.* 101, 112906 (2012).
14. T.M. Tsai, K.C. Chang, T.C. Chang, Y.E. Syu, S.L. Chuang, G.W. Chang, G.R. Liu, M.C. Chen, H.C. Huang, S.K. Liu, Y.H. Tai, D.S. Gan, Y.L. Yang, T.F. Young, B.H. Tseng, K.H. Chen, M.J. Tsai, C. Sze, H. Sze, and S.M. Sze, *IEEE Electron Device Lett.* 33, 1696 (2012).
15. T.M. Tsai, K.C. Chang, T.C. Chang, G.W. Chang, Y.E. Syu, Y.T. Su, G.R. Liu, K.H. Liao, M.C. Chen, H.C. Huang, Y.H. Tai, D.S. Gan, C. Ye, H. Wang, and S.M. Sze, *IEEE Electron Device Lett.* 33, 1693 (2012).
16. A. Marcus, E.H. Keith, L. Michael, U.S. Patent No. 3,886,578. (1975).
17. F.W. Yang, K.H. Chen, C.M. Cheng, and F.Y. Su, *Ceram. Int.* 39, S729 (2013).
18. K.H. Chena and C.F. Yang, *Ferroelectrics* 381, 1 (2009).
19. K.H. Chen, Y.C. Chen, Z.S. Chen, C.F. Yang, and T.C. Chang, *Appl. Phys. A, Mater. Sci. Process.* 89, 533 (2007).
20. T.Y. Tseng and H. Nalwa, *Handbook of Nanoceramics and Their Based Nano Devices*, Vol. 175 (Los Angeles: American Scientific Publishers, 2009).
21. R. Ghosh, G.K. Paul, and D. Basak, *Mater. Res. Bull.* 40, 1905 (2005).